Bio-Design and Manufacturing (2026) 9:122–136
https://doi.org/10.1631/bdm.2500291

RESEARCH ARTICLE

Bioextrusion of hydrogels with controlled mineral gradients for regenerative engineering of osteochondral interfaces

Xiao Zhao[1] · Weiwei Wang[2,3] · Xiaojun Yu[2] · Dilhan M. Kalyon[1] · Cevat Erisken[4]

Received: 7 June 2025 / Accepted: 9 October 2025 / Published online: 16 December 2025

Abstract

The osteochondral (OC) interface exhibits a mineral gradient, varying in thickness by several hundred micrometers across different species. Disruptions in this interface damage OC tissues, leading to osteoarthritis. The natural architecture and composition of native OC interfaces can be replicated using biomaterial scaffolds via regenerative engineering approaches. A novel one-step bioextrusion process was employed to fabricate a unitary synthetic graft (USG), which mimics the native OC interface's mineral concentration gradient. This novel USG is composed of an agarose-based cartilage layer and a bone layer, consisting of agarose enriched with 20% (200 g/L) hydroxyapatite. The USG features a gradient interface with mineral concentrations transitioning from 0% to 20% (mass fraction), mimicking the transition between the cartilage and bone. Thermogravimetric analysis revealed that the gradient transition lengths of the graft and native OC tissue harvested from bovine knees were similar ((647±21) vs. (633±124) μm). The linear viscoelastic properties of the grafts, which were evaluated using strain sweep and frequency sweep tests with oscillatory shear, indicated a dominant storage modulus over loss modulus similar to that of native OC tissues. The compressive and stress relaxation behaviors of the USGs demonstrated that the graft maintained structural integrity under mechanical stress. Viability assays performed after bioextrusion showed that chondrocytes and human fetal osteoblast cells successfully integrated and survived within their designated regions of the graft. The novel USGs exhibit properties similar to native OC tissue and are promising candidates for regenerating OC defects and restoring knee joint functionality.

Dilhan M. Kalyon and Cevat Erisken have contributed equally to this work.

✉ Dilhan M. Kalyon
dkalyon@stevens.edu

✉ Cevat Erisken
cevat.erisken@nu.edu.kz

[1] Department of Chemical Engineering and Materials Science, Charles V. Schaefer, Jr. School of Engineering & Science, Stevens Institute of Technology, Hoboken, NJ 07030, USA

[2] Department of Biomedical Engineering, Charles V. Schaefer, Jr. School of Engineering & Science, Stevens Institute of Technology, Hoboken, NJ 07030, USA

[3] School of Life Sciences, Yantai University, Yantai 264006, China

[4] Department of Chemical and Materials Engineering, School of Engineering and Digital Sciences, Nazarbayev University, Astana 010000, Kazakhstan

Graphical abstract

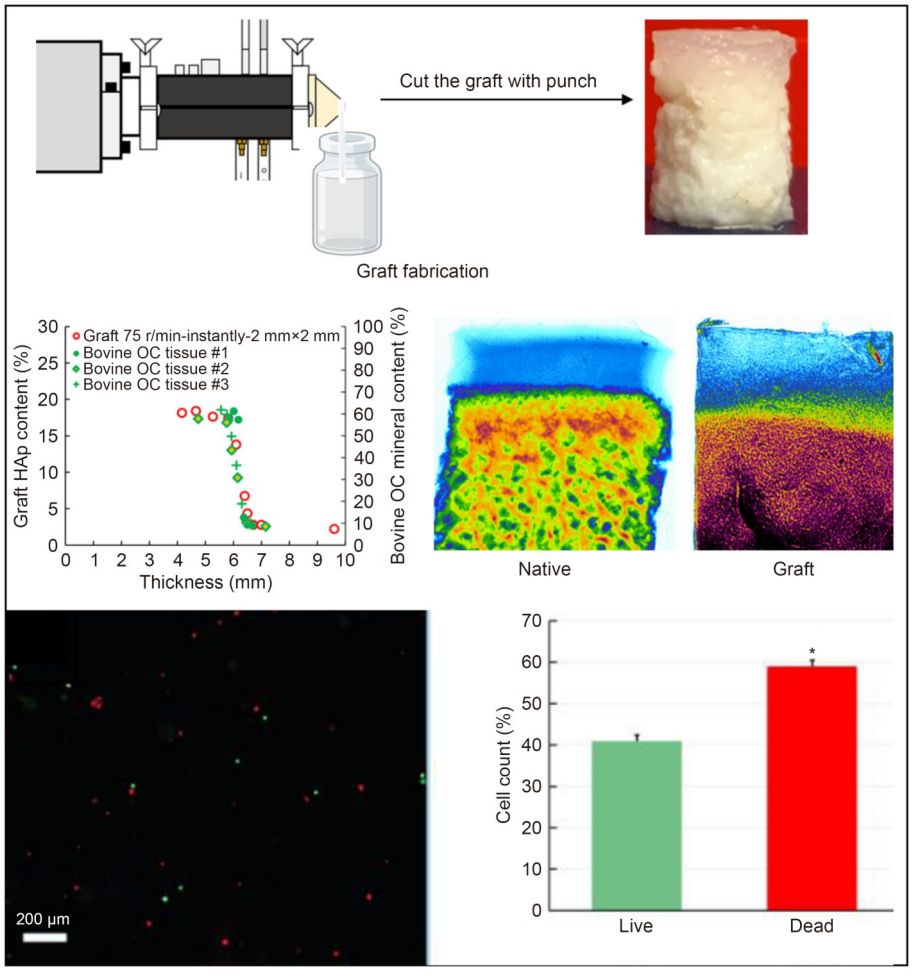

Keywords Osteochondral (OC) interface · Mineral gradient · Bioextrusion · Hydrogel scaffold · Regenerative engineering

1 Introduction

Knee joint function is compromised by osteochondral (OC) tissue damage due to age-related degeneration, mechanical trauma, and other pathological conditions [1]. Untreated OC damage causes osteoarthritis (OA), which usually occurs in individuals over 50 years old. More than 528 million people worldwide develop OA [2], causing an economic burden of approximately 136.8 billion dollars [3]. Currently, OA is treated surgically using microfracture, mosaicplasty, and either extracellular matrix (ECM)-based or synthetic grafts [4]. Unfortunately, the biological connections between the grafts and the native tissues are poor, or a mechanically weaker fibrocartilage tissue develops. Therefore, there is an unmet demand for designing and fabricating new synthetic or biological grafts that are more similar to native tissue, in terms of composition, structure, and function.

OC tissue is located at the end of long bones and consists of three different but continuous layers: unmineralized cartilage (articular cartilage), mineralized cartilage (calcified cartilage), and subchondral bone [5, 6]. These layers form a graded structure from articular cartilage to subchondral bone [7, 8] (Fig. 1). Successful replication of this complex graded OC tissue requires equally complex technologies to fabricate the gradations in grafts. These technologies should address the graded tissue transitions found in human tissues, including the interfaces between cartilage and bone, ligament and bone, and tendon and bone [9–12]. Some of these technologies are amenable to scaling up to industrial fabrication levels under controlled and reproducible conditions. For example, several extrusion-based

fabrication methods are suitable for the fabrication of graded scaffolds [13–16].

Various biocompatible materials, including natural polymers, synthetic polymers, and combinations of these polymers [17, 18], have been employed to fabricate scaffolds for OC tissue. Scaffolds may also be fabricated using decellularized tissues [19]. Agarose is a well-characterized hydrogel widely used as a matrix for chondrocyte bioactivity and cartilage tissue engineering [20, 21]. Chondrocyte-laden agarose constructs exhibit physiologically relevant mechanical properties approaching the properties of native cartilage [22]. Hydroxyapatite (HAp) is present in bone tissue and is commonly used for bone tissue regeneration. Incorporating HAp into hydrogels improves the mechanical properties and bioactivity of 3D-printed scaffolds [23, 24].

The aims of this study were (i) to characterize the OC interface of the bovine knee, focusing on the unique structural and mineral components, (ii) develop a continuously graded unitary synthetic graft (USG) that replicates the structural properties of a native OC interface using agarose and HAp as the primary biomaterials, and (iii) employ bioextrusion technology to fabricate a USG with graded calcium content similar to natural OC tissues. We hypothesized that a hydrogel-based graft made with bioextrusion would closely resemble the structural and compositional attributes of a native OC interface. This is a novel approach to simulating the physiological characteristics of calcium gradients within OC tissues.

The results of this study provide valuable insights into the application of biomaterials to OC repair and regeneration in both preclinical and translational settings. These insights will significantly advance orthopedic research, potentially influencing the technological and socio-economic aspects of the field. This novel approach can be used to develop grafts with similar physiological and structural characteristics as native tissues to address the lack of effective OC regeneration solutions for the rapidly aging global population.

2 Materials and methods

The experimental procedure is shown in Fig. 2. First, OC tissues from bovine knee joints were harvested and

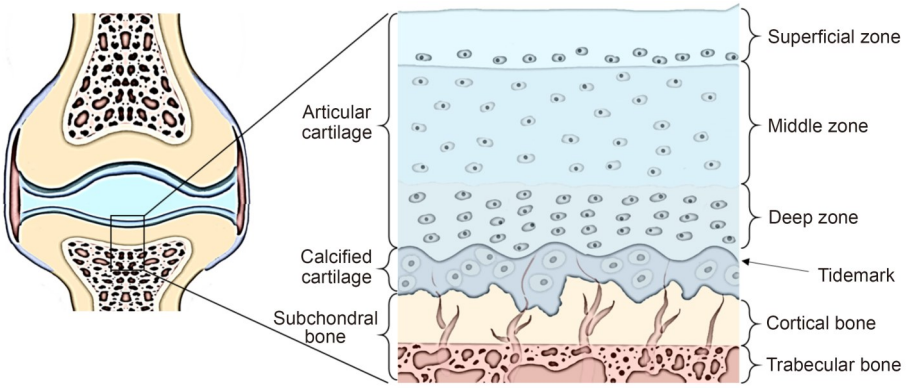

Fig. 1 Structural representation of the OC tissue (layer thicknesses are not to scale)

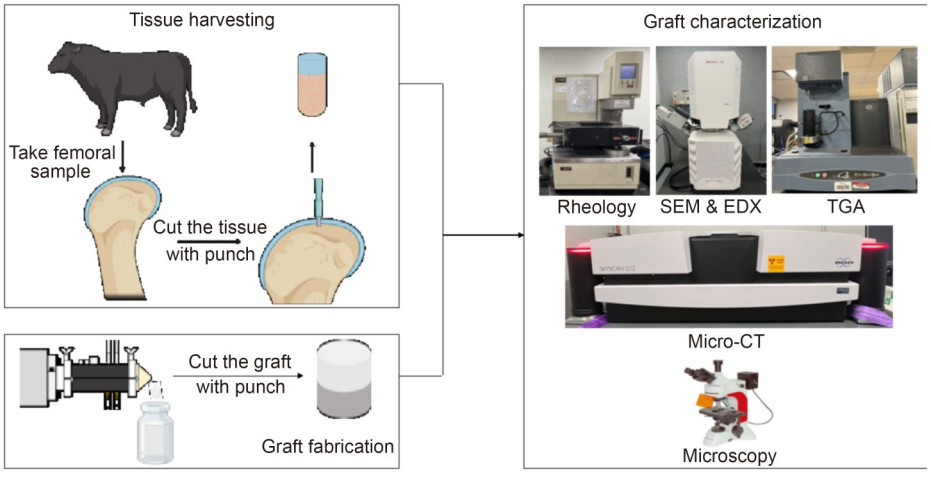

Fig. 2 Experimental procedure for tissue harvesting, graft fabrication, and graft characterization. SEM: scanning electron microscopy; EDX: energy-dispersive X-ray; TGA: thermogravimetric analysis; Micro-CT: micro-computed tomography

characterized. Second, grafts were printed and characterized. Third, the distribution of mineral content and the biomechanical and rheological properties of the grafts were compared with the OC tissues from bovine knees. Fourth, the viability of extruded chondrocytes and human fetal osteoblasts (hFOBs) in hydrogel was investigated.

2.1 Materials

Low-melting-temperature agarose was obtained from Cambrex Bio Science Rockland (Product #50100, Rockland, ME, USA). HAp (Product #04238) and phosphate-buffered saline (PBS, Product #524650) were obtained from Sigma-Aldrich (Saint Louis, MO, USA). Detailed sources of biological materials are specified in the appropriate sections of the manuscript.

2.2 Harvesting the OC tissue

Bovine knee joints (1–2 years old, n=3) were obtained from a local slaughterhouse and stored at 4 °C. The refrigerated knee joints were brought to room temperature before testing, and plugs were harvested from the femoral condyle using 4- and 8-mm punches (Fig. 3). The mineral content was evaluated in the 4-mm specimens using thermogravimetric analysis (TGA). Micro-computed tomography (micro-CT) and biomechanical and rheological measurements were performed using the 8-mm specimens.

2.3 Formulation and extrusion printing of graded OC grafts

The USG was fabricated to include a chondrogenic region, a transition region, and a bone region. Agarose was dissolved in PBS solution at a concentration of 0.02 g/mL to prepare the chondrogenic hydrogel. The solution was heated to boiling three times to ensure complete polymerization. HAp nanoparticles were added to the 2% agarose solution to make a 20% solution (0.2 g HAp per milliliter of 2% agarose), and the solution was sonicated after mixing to disrupt agglomerates. The agarose and agarose/HAp mixtures were non-flowable at room temperature but transformed into injectable fluids at ≥37.5 °C before addition to the extruder via infusion pumps. The agarose solution and agarose/HAp suspension solidified into gels at room temperature to make the OC USGs (Fig. 4).

Functionally graded biomimetic USGs were fabricated using a twin-screw extruder with fully intermeshing, co-rotating 7.5 mm diameter screws, custom-built by Material Processing and Research, Inc. (New Jersey, USA). The extruder was equipped with a slit die tailored specifically for this application (die dimensions in Table 1). Multiple feeding ports allowed the continuous introduction of solutions/suspensions, including the agarose solution and the agarose/HAp suspension. The extruder screws enhanced dispersive mixing, breaking up agglomerates of HAp that formed

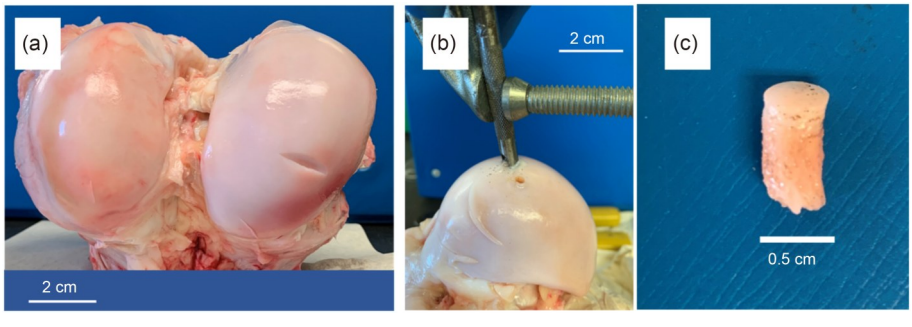

Fig. 3 Harvesting and preparation of OC tissue. (a) Gross view of bovine femoral condyles. (b) Specimen collection using 4-mm and 8-mm punches. (c) Specimens for thermogravimetric (4 mm), micro-CT, biomechanical, and rheological characterization (8 mm)

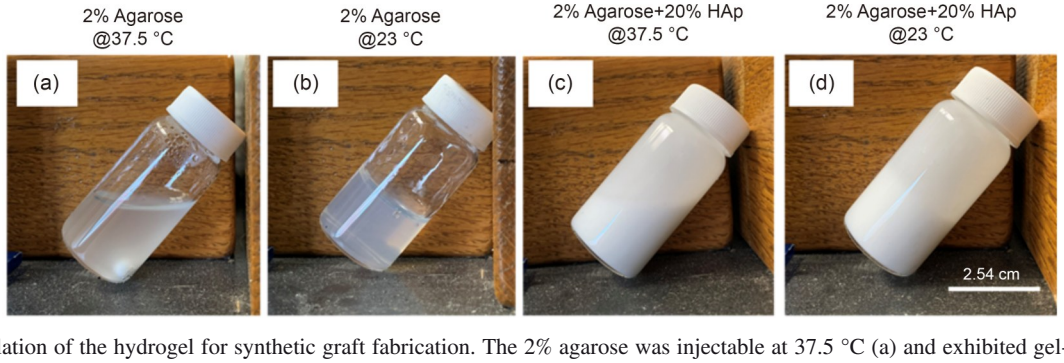

Fig. 4 Formulation of the hydrogel for synthetic graft fabrication. The 2% agarose was injectable at 37.5 °C (a) and exhibited gel-like behavior at room temperature (b). Similarly, the 20% HAp suspension was injectable at 37.5 °C (c) and gel-like at room temperature (d)

Table 1 Parameters used to optimize the gradient transition length

Run index	Lag time (s)	Rotational speed (r/min)	Die opening (width× height; mm×mm)
1	30	50	10×3
2	12	50	10×3
3	0	75	2×2

during initial mixing. Combinations of kneading disks and fully flighted elements were staggered at specific angles and directions to optimize distributive and dispersive mixing efficiency [25–28].

The twin-screw extruder was housed in an environmental chamber maintained at 37.5 °C. The barrel temperature was maintained at 37.5 °C by circulating water through a heated bath (Figs. 5a and 5b). This setup prevented the premature gelation of the agarose and agarose/HAp suspensions during processing. The agarose solution was introduced through an injection point near the die, and the agarose/HAp suspension was fed through a different injection point. HAp concentrations within the OC USG were continuously varied from 0% to 20% (by weight) by adjusting the agarose and agarose/HAp feed rates in a time-dependent manner. The overall feed rate to the extruder was maintained at 10 mL/h. The flow rate of agarose was incrementally increased from 0 to 10 mL/h at 1.5 mL/h intervals, while the flow rate of the agarose/HAp was decreased from 10 to 0 mL/h at 1.5 mL/h intervals. The gradient formation within a specific length was controlled by varying the lag time between feed rate adjustments, the rotational speed of the screws, and the die opening. The impact of these adjustments on the gradient distance and the optimized parameters for achieving the desired grading distance are shown in Table 1.

The agarose and agarose/HAp under the conditions defined in Table 1 were extruded into 25-mm vials, which were moved from the environmental chamber to room temperature to form the USG. These grafts were punched into cylindrical shapes for thermogravimetric, mechanical, rheological, micro-CT characterization, and microscopic visualization. For scanning electron microscopy (SEM) and energy-dispersive X-ray (EDX) characterizations, the specimens were cut into rectangular shapes for better imaging.

2.4 Thermogravimetric characterization of OC tissue and grafts

The weight fraction of mineral content in the native OC tissues and the HAp content in the USGs were validated using a TGA (TGA-Q50, TA Instruments, New Castle, Delaware, USA). The tissues were harvested from femoral condyles, and the tissues and USGs were stored in sealed packages at 4 °C in a hydrated chamber during sample collection to prevent dehydration. Slices were cut from the cylindrical tissues and grafts, and the thickness was measured using a digital caliper (AOS 500, Mitutoyo, Japan). The sections were placed in the analyzer's sampler. The residues of the sliced specimens were determined after heating from 25 to 550 °C at a rate of 25 °C/min under nitrogen.

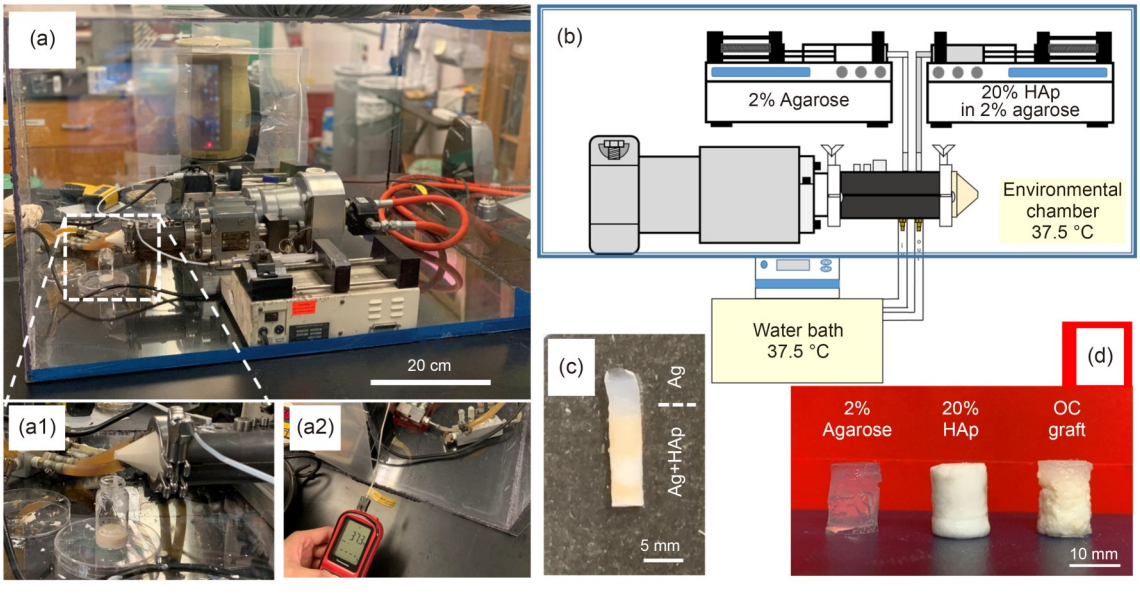

Fig. 5 Bioextrusion of OC grafts. OC grafts contained HAp at the bottom, a continuously decreasing concentration of HAp (from 20% to 0%) in the middle, and pure agarose at the top, designed to mimic bone, OC interface, and cartilage, respectively. (a, b) Grafts were fabricated using a twin-screw mini extruder installed in an environmental chamber. The 2% agarose solution and agarose/HAp were fed into the extruder from two separate infusion pumps with changing flow rates to create a gradient of HAp. Graft specimens were formed using 4 mm (c) and 8 mm (d) punches for thermogravimetric, rheological, and micro-CT characterizations

2.5 SEM and EDX characterization

The OC tissues and USGs were freeze-dried overnight, coated with gold, and imaged using an SEM (Scientific Apreo 2, Thermo Fisher, USA). The EDX of the OC grafts was conducted under SEM after scanning for 300 s at 20 kV to validate the presence of calcium and phosphorus.

2.6 Biomechanical characterization of OC tissue and grafts

The compressive properties of OC tissues and USGs were characterized using a rheometer (ARES, Rheometric Scientific, currently TA Instruments) in the strain range of 0%–5% at a constant compression rate of 0.05 mm/s while immersed in 37 °C PBS. This strain level was previously used for biomechanical characterizations of native cartilage and engineered tissues [7, 29]. The specimens were initially subjected to a normal force (0.03 N) to obtain full contact before initiating the compression test.

2.7 Linear viscoelastic properties and relaxation of OC tissue and grafts

Compression and the oscillatory shear of the samples were characterized using the ARES rheometer. The native tissue or graft specimens were inserted between two disks (8 mm diameter) immersed in 37 °C PBS to prevent drying during the experiments [29]. The upper disk was either oscillated in the clockwise and counterclockwise directions or translated in the downward direction at a constant velocity, and the second disk, which remained stationary, was connected to the torque and normal force transducer.

In the small-amplitude oscillatory shear test, the shear strain oscillated as a function of time as Eq. (1):

$$\gamma=\gamma_0\sin(\omega t), \tag{1}$$

where γ_0 is the shear strain amplitude (i.e., $\theta D/h$, with θ being the angular displacement, D the disk diameter, and h the gap between the two disks), ω is the oscillation frequency, and t is time. The shear stress (τ) response to the oscillatory deformation consisted of two components related to the stored energy and energy dissipated as heat, according to Eq. (2):

$$\tau=G'(\omega)\gamma_0\sin(\omega t)+G''(\omega)\gamma_0\cos(\omega t), \tag{2}$$

where $G'(\omega)$ is the shear storage modulus and $G''(\omega)$ is the shear loss modulus. The ratio of $G''(\omega)$ to $G'(\omega)$ is $\tan\delta$. The oscillatory shearing was conducted in the linear viscoelastic region where the moduli were independent of the strain amplitude. The strain amplitude sweeps indicated that up to a strain amplitude of 0.1%, the oscillatory shear deformation of the hydrogels and the native tissue occurred in the linear region. The dynamic properties $G'(\omega)$ and $G''(\omega)$ were characterized as a function of the frequency range of 0.1–100 rad/s at 0.1% strain. The linear viscoelastic response of the tissue over a range of time scales was performed by sweeping the frequencies. The elastic response was emphasized at relatively short characteristic deformation times, and the viscous flow behavior was emphasized at longer characteristic times. Time sweep tests performed earlier on cartilage tissue [29] and hydrogels [30] suggested that the samples were stable within the time scale of the experiments, which was usually less than 15 min of shearing per sample.

2.8 Micro-CT characterization of OC tissue and grafts

The bovine OC tissue samples were harvested from the bovine knee joint and immediately tested. The samples were kept hydrated with a customized moisture chamber during the testing. The graft specimens were tested after freeze-drying in air. The micro-CT machine (SkyScan 1272, Bruker, MA, USA) was operated at the following parameters: source voltage, 60 kV; source current, 70 μA; 2×2 binning; Al filter, 0.5 mm; resolution, 2048×2048 with varied pixel sizes. The 3D reconstruction of bone mineral density was performed using the built-in micro-CT software set (CTVox and CTAn) from Bruker.

2.9 Bioextrusion of hFOBs and chondrocytes

hFOBs (Catalog# CRL-3602, TCC, USA) and rat articular cartilage chondrocytes (Cells-Online LLC, USA) were used for the bone and cartilage regions of the USG, respectively. All cells were incubated at 37 °C and 5% CO_2. The hFOBs were maintained in a 1:1 mixture of Ham's F12 medium and Dulbecco's modified Eagle's medium (DMEM), supplemented with 2.5 mmol/L L-glutamine, 1% antibiotics (penicillin/streptomycin), and 10% fetal bovine serum. The medium was changed every 2 d. The hFOB cells (20 mL of 3.0×10^4 cells/mL) were labeled with green CMFDA (#C7025, Thermo Fisher), mixed with 20 mL of agarose/HAp suspension, and fed into the extruder unit for bioextrusion. Rat articular cartilage chondrocytes were cultured in DMEM supplemented with 10% fetal bovine serum and 1% penicillin/streptomycin. The medium was changed every other day. Agarose hydrogel scaffolds were prepared in sterilized PBS. Chondrocytes (10 mL of 3.0×10^4 cells/mL) were mixed with 10 mL of 2% agarose (0.02 g agarose/mL PBS) and fed into the extruder for bioextrusion. Before infusing the hydrogels into the extruder, chondrocyte cell viability

was determined at different concentrations of agarose (0.5%–2%).

After warming the CellTracker™ Green CMFDA (#C7025, Thermo Fisher) to room temperature, a 10 mmol/L stock solution of green CMFDA in dimethyl sulfoxide (DMSO) was prepared. The stock solution was diluted to a working concentration of 5 μmol/L for labeling. After removing the culture medium, the pre-warmed working solution was added, and the cells were incubated for 30 min at 37 °C in a 5% CO_2 incubator. After removing the working solution, the cell culture medium was added as described above. The stained cells were visualized using a fluorescent microscope (emission: 514 nm; excitation: 485 nm) for 72 h.

For bioextrusion of cells, chondrocytes were mixed with 2% agarose, and hFOBs were mixed with 20% HAp/agarose (0.2 g HAp per milliliter of 2% agarose). The mixtures were fed into the extruder, and the cellular OC graft was formed according to the conditions described in Sect. 2.3. The bottom part of the bioextruded construct, containing hFOBs, mimicked the bone part, and the top part, containing chondrocytes, mimicked the cartilage. Cylindrical specimens were punched and processed for staining and imaging. The hFOB cells were already labeled as previously described. One drop of 4′,6-diamidino-2-phenylindole (DAPI) solution was added to the sections to stain the cell nuclei before imaging.

To section the OC grafts, the samples were incubated in 15% or 30% (0.15 or 0.30 g/mL) sucrose in PBS and embedded in optimal cutting temperature compound. The specimens were sectioned into 8-μm-thick slices with a cryostat microtome. The mineralized matrix within the grafts was analyzed using Alizarin Red staining. Sections were rinsed with PBS, fixed in 10% neutral buffered formalin for 30 min, and stained with 2 mL of 40 mmol/L Alizarin Red S (TMS-008-C, Millipore, Germany) for 30 min under gentle agitation. The sections were rinsed 10 times with deionized water to remove non-specific binding. The sections were imaged using a stereomicroscope (T100, Nikon, Japan). Fluorescent imaging was performed utilizing CMFDA for green staining and DAPI for blue staining of the cell nuclei. Fluorescently labeled cells were imaged using a stereomicroscope (SMZ1500, Nikon).

2.10 Statistical analysis

The thicknesses of the gradients in the native OC and the grafts were compared using Student's *t*-tests. The modulus of the graft and the first and second moduli of the native tissue were compared using one-way analysis of variance (ANOVA). A p value <0.05 was considered statistically significant.

3 Results

3.1 Gradient transition length determined by TGA

The gradient transition length is the length over which the HAp concentration changes from high to low (from bone to cartilage). Two sets of experiments were performed using TGA. First, the mineral content of the bovine OC tissue was analyzed across the bone–cartilage interface. Second, variations in HAp concentration across the bone to cartilage transition in the printed USGs were quantified. The harvested bovine OC tissues were approximately 10 mm thick. The cartilage and OC layers together were approximately 2 mm. Thus, assessments were conducted up to 3 mm from the articular surface.

Based on TGA measurements, the gradient transition length for the native OC tissue was (633±124) μm (Fig. 6a, n=3). The USGs formed under the conditions specified in Table 1 exhibited different gradient transition lengths (Fig. 6b). Reducing the time between flow rate changes from 30 to 12 s decreased the gradient transition length from 3830 to 2720 μm. Instantaneously altering the flow rate, increasing the screw rotational speed, and reducing the die opening decreased the gradient transition length to (647±21) μm. As shown in Fig. 6c, the gradient transition lengths of the OC tissue and the USG, measured using TGA characterization, were similar. Comparison is given in Fig. 6d ($p>0.05$).

3.2 SEM and EDX characterization

The SEM imaging, EDX elemental mapping, and line scan analyses qualitatively and semi-quantitatively demonstrated similar mineral distributions in the native OC tissue and the USGs. Changes in tissue and graft composition as a function of distance from the surface were indicated by the color differences in the gross images (Figs. 7a1 and 7b1). Structural and compositional (as calcium content) changes were demonstrated by SEM (Figs. 7a2 and 7b2) and EDX (Figs. 7a3, 7a4, 7b3, and 7b4).

Calcium was absent on the surfaces of the OC tissue and the USG. The calcium concentration gradually increased in the cartilage–bone transition region, and then remained constant. The changes in calcium content were quantified, as shown in Figs. 7c1–7c3. The thickness of the native OC interface gradient was approximately 140 μm, based on the median values in the violin plot (Fig. 7c2) and around 275 μm based on the mean values in the scatter plot (Fig. 7c1). The OC native tissue and graft exhibited gradual changes in calcium content at the interface region.

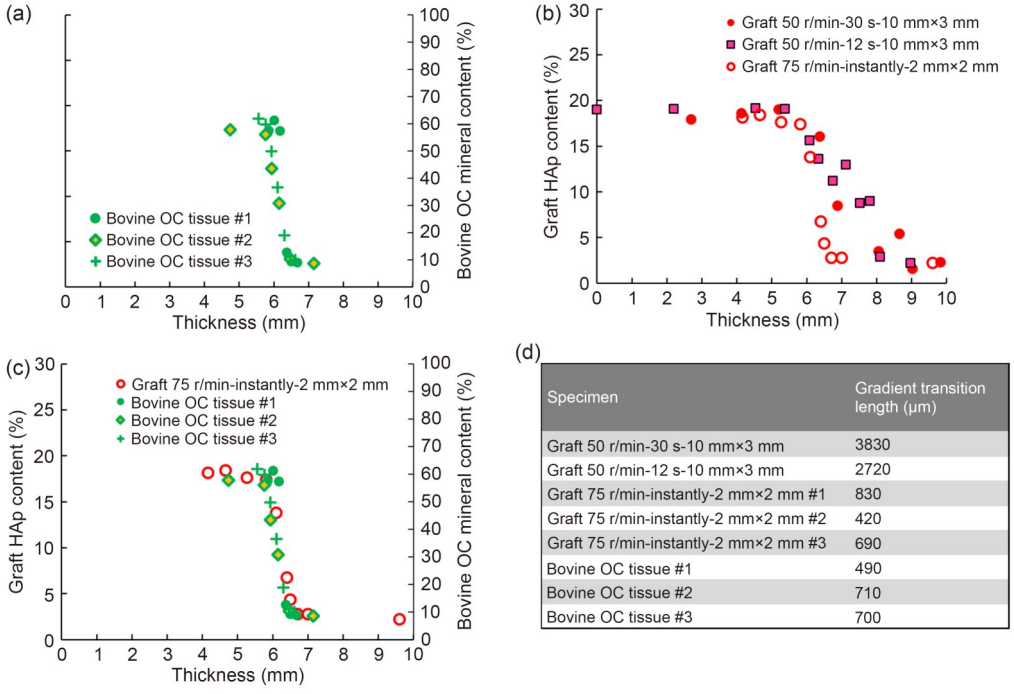

(d)

Specimen	Gradient transition length (μm)
Graft 50 r/min-30 s-10 mm×3 mm	3830
Graft 50 r/min-12 s-10 mm×3 mm	2720
Graft 75 r/min-instantly-2 mm×2 mm #1	830
Graft 75 r/min-instantly-2 mm×2 mm #2	420
Graft 75 r/min-instantly-2 mm×2 mm #3	690
Bovine OC tissue #1	490
Bovine OC tissue #2	710
Bovine OC tissue #3	700

Fig. 6 Determination of the mineral gradient in bovine OC tissue (a) and USGs (b) and comparison of the two specimens (c, d). (a) The mineral concentration of the bovine OC tissue (approximately 10 mm thick) was determined as a function of the thickness of the tissue (n=3). The bottom and top parts of the OC tissue corresponded to bone and cartilage, respectively. (b) Process parameters (screw rotational speed and lag time) and extruder design parameters (die dimensions) were adjusted to form a gradient of HAp in the graft similar to native OC tissue. (c) The gradient transition lengths in the OC tissue and graft overlapped. (d) The gradient transition lengths for grafts fabricated under different conditions and bovine OC tissue

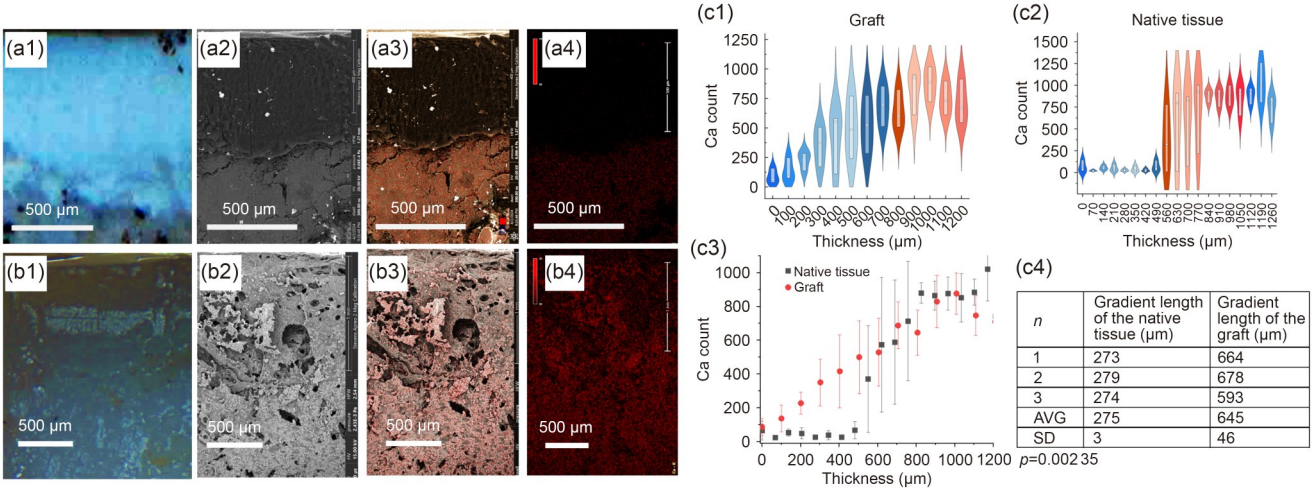

(c4)

n	Gradient length of the native tissue (μm)	Gradient length of the graft (μm)
1	273	664
2	279	678
3	274	593
AVG	275	645
SD	3	46

Fig. 7 A gross image (a1), SEM micrograph (a2), and calcium mapping (a3, a4) of fresh bovine OC tissue. A gross image (b1), SEM micrograph (b2), and calcium mapping (b3, b4) of the OC graft (USG). (c1–c3) The grading distances for native OC tissue and the grafts determined by line scans over the EDX-mapped images and (c4) the corresponding gradient lengths (n=3). Error bars represent standard deviations

3.3 Linear viscoelasticity and biomechanical properties of the OC tissue and grafts

The linear viscoelastic material functions of the USGs and native OC tissues were characterized using an ARES rheometer. Oscillatory shear experiments were conducted to evaluate sample stability under shear, determine the strain amplitude range for linear behavior, and determine the dependence of storage and loss moduli on deformation rates (frequency). An initial time sweep test of approximately 15 min was conducted to verify data reliability. The results indicated stable properties. The storage modulus was measured over 900 s (Fig. 8a). No significant temperature sensitivity was detected in the tissues and grafts between 19 and 39 °C (Fig. 8b).

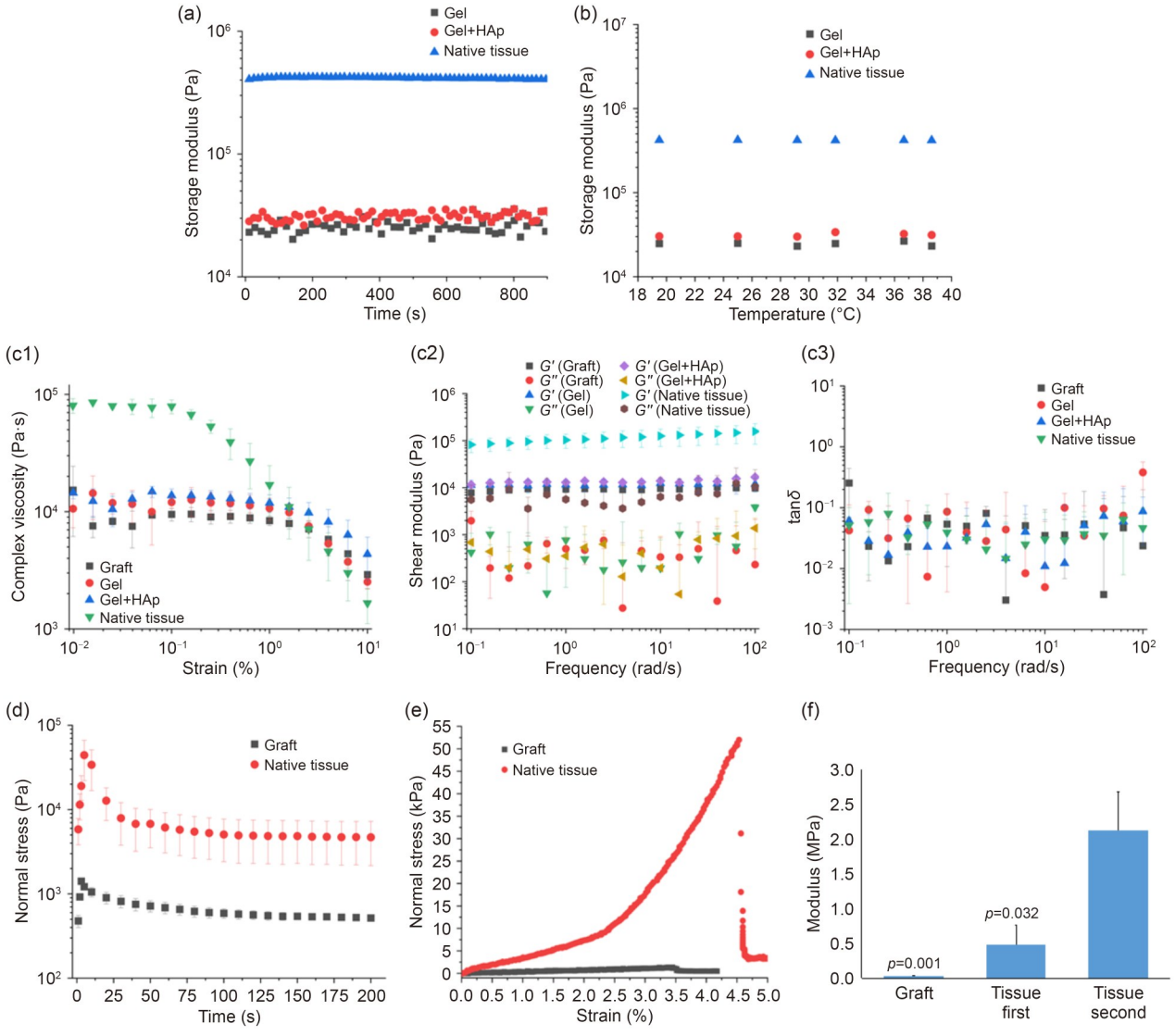

Fig. 8 Linear viscoelastic material functions and compressive properties of bovine OC tissue and the USG (graft). (a) Time sweep of the native tissue (Gel: agarose gel alone; Gel+HAp: agarose gel with hydroxyapatite). (b) Temperature sweep of the OC tissue. Strain sweep at 1 rad/s (c1), frequency sweep behavior at 37 °C (c2), and tanδ (c3) of native OC tissue and USGs. (d) Relaxation behavior of the OC tissue and USGs. (e) Stress–strain behavior of the USG and the OC tissue with two moduli. (f) Compressive moduli of the OC tissue and graft. Error bars represent standard deviations, and p-values show comparisons with the second modulus of the OC tissue

A strain sweep test was used to determine the linear viscoelastic range for each sample. The native OC tissues exhibited consistent rheological properties up to a 0.1% strain amplitude, whereas the grafts and their components (agarose and agarose/HAp) maintained stable properties up to a 1% strain amplitude (Fig. 8c1). Thus, the frequency sweep test was conducted at 0.1% strain, where the OC tissues and all graft compositions displayed typical gel-like behavior. This is indicated by frequency-independent responses in storage (G') and loss (G'') moduli (Figs. 8c2 and 8c3); the storage modulus significantly exceeded the loss modulus, as indicated by tanδ values below 1 (Fig. 8c3).

The compression stress relaxation behavior was analyzed by imposing 5% compression over 2 s (Fig. 8d). After the initial strain, normal stress in the native OC tissues and grafts gradually decreased. The time-dependent relaxation was characterized by a gradual decrease in normal stress, which stabilized around 200 s. The native tissues and the USGs behaved similarly, highlighting the successful replication of native tissue viscoelastic properties in the USGs.

Figures 8e and 8f show the compressive stress–strain behavior of the native OC tissue and the graft. The native OC tissue exhibited dual moduli. The initial modulus, representing the cartilage region, was recorded at (0.48±0.28) MPa, and the second modulus, indicative of the bone region, was recorded at (2.13±0.55) MPa (p<0.05 vs. the initial modulus). Conversely, the OC graft exhibited consistent linear stress–strain behavior until failure. The modulus of the graft

((0.04±0.01) kPa) was notably lower than the second modulus of the native tissue ($p<0.05$).

3.4 Micro-CT characterization of OC tissue and grafts

Native OC tissue specimens and grafts were examined using micro-CT imaging, and the mineral density was measured by dividing the entire specimen into 12–14 μm layers. The specimen images show the cartilage, bone, and the transition between the two (Figs. 9a and 9b). The changes in bone mineral density of the specimens were plotted as a function of length from the first value where a signal was detected (individual runs shown in Fig. 9c1 and means with standard deviations in Fig. 9c2).

3.5 Bioextrusion of hFOBs and chondrocytes

A twin-screw extruder was used to bioprint the agarose hydrogel containing chondrocytes and agarose/HAp hydrogel containing hFOBs. The final cellular USGs were then visualized (Fig. 10). As shown in Fig. 10a, the chondrocytes were viable in Ag hydrogel concentrations ranging from 0.5% to 2%, with reduced survival after 1.5%. For the bioextrusion process, a 2% Ag concentration was chosen based on its favorable biomechanical properties. Post-bioextrusion survival of chondrocytes and hFOBs was confirmed (Figs. 10b and 10c). The graded mineralization within the OC grafts is visible in Fig. 10d. These results demonstrate the effective incorporation and distribution of minerals in the bioextruded structures.

4 Discussion

Fabricating scaffolds or grafts that accurately replicate the complex structure and precise mineral gradients of native OC tissue poses significant challenges. The main objective of this study was to engineer a graft that mimics the mineral gradient in native OC tissue. To achieve this goal, we employed extrusion printing to construct grafts made from agarose solutions with and without HAp. These solutions were fed through two separate ports of the extruder. The mineral gradient was carefully engineered by adjusting the flow rates of the agarose solution and the agarose/HAp suspension to ensure a consistent overall flow rate. Several parameters, including the rotational speed of the screws, the die opening, and the timing of flow rate changes, were adjusted to refine the gradient transition length from 5 mm to <700 μm. These adjustments resulted in a gradient transition length similar to native OC tissue, as determined by TGA. The optimal settings included a rotational speed of 75 r/min, a die

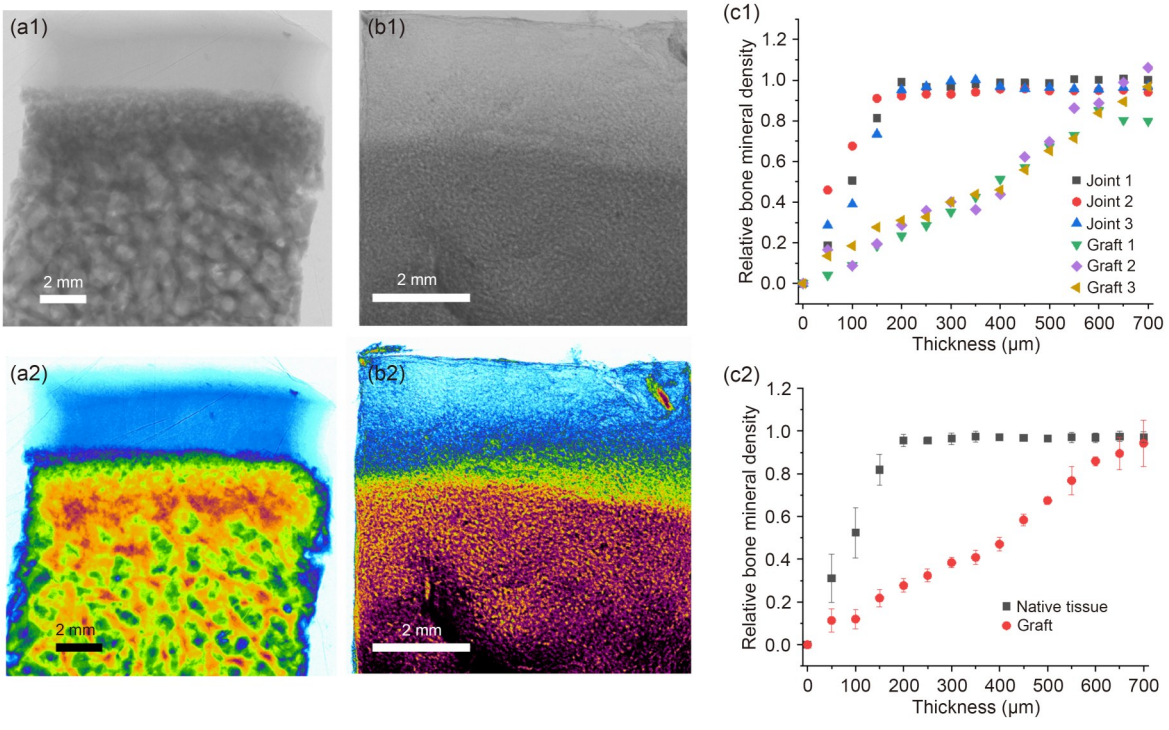

Fig. 9 Micro-CT characterization of OC tissue (a) and the USG (b), and grading length for OC tissue (Joint) and the USG (c). The native OC tissue and the graft were imaged using micro-CT (a1, b1) and colored for better visualization (a2, b2). (c1, c2) The specimens were scanned in layers for mineral density, processed, and plotted for comparison. (c2) is the average of the data reported in (c1). Error bars in (c2) represent standard deviations

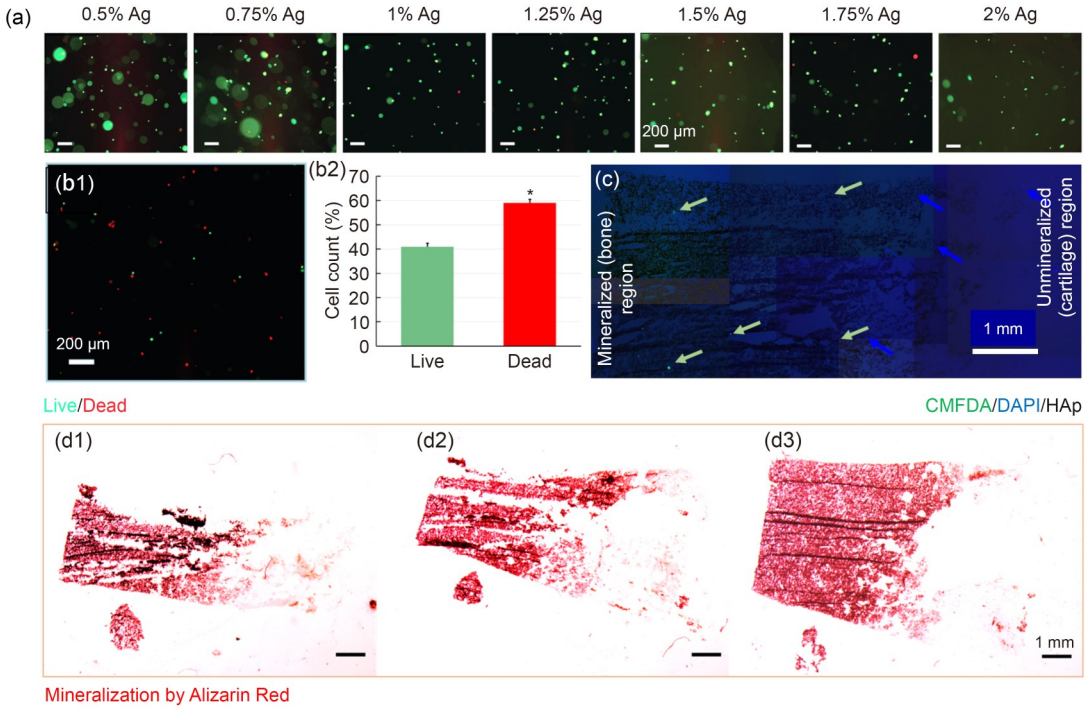

Fig. 10 Bioextrusion of hFOBs and chondrocytes. (a) Survival (live/dead stain) of chondrocytes in different concentrations of Ag gels (0.5%–2%) before bioextrusion. (b) Live/Dead staining of chondrocytes (3×10^4 cells/mL) in 2% Ag after bioextrusion. (c) Stereomicroscope image of CMFDA-labeled hFOBs and (d) Alizarin Red staining of the mineralized matrix (different grafts obtained from different runs). The green arrows in (c) point to CMFDA-labeled hFOBs, the blue arrows represent DAPI staining, and the black color represents HAp. $^*p<0.05$. See the supplementary information for a higher magnification of (c). Data in (b2) are expressed as mean±standard deviation ($n=3$)

opening of 2 mm×2 mm, and precise switching between flow rates to achieve the desired gradient.

After testing a range of agarose concentrations, 2% agarose and 20% HAp were identified as the optimal concentrations (Fig. 10a). Cell survival decreased in agarose solutions greater than 1.5% concentration. To improve the mechanical properties of the graft, 2% agarose was selected. A recent study using 3D printing demonstrated the feasibility of 3.5% HAp in a GelMA-based graft [31]. Utilizing an extruder enabled us to go to a relatively high HAp level of 20%. However, this value is lower than the mineral concentration in native OC tissue (approximately 60% by weight, Fig. 6c) and requires further consideration. TGA was employed to quantify the HAp content within the composite USGs. TGA can differentiate between organic material decomposition and residual inorganic content, which primarily consists of HAp that is stable at up to 550 °C [15]. The analysis confirmed that approximately 20% of the material did not decompose, indicating the presence of HAp.

The linear viscoelastic properties of the USGs were characterized under oscillatory shear and compared with native OC tissue. The storage moduli for the grafts and native OC tissue were independent of time and temperature. The tanδ values demonstrated that the tissue and USG exhibited frequency-independent gel-like behavior, with storage moduli significantly exceeding loss moduli. After compression, the USGs and native OC tissue exhibited incomplete stress relaxation over 200 s, highlighting the significant role of viscoelasticity. Unlike Newtonian fluids, in which the stress decays instantly upon cessation of shearing, or purely elastic materials that maintain constant stress under sustained strain, the USGs and native OC exhibited typical viscoelastic stress relaxation.

Differences in biomechanical properties between the USGs and native OC tissue were detected. Although native OC tissue exhibited a two-slope stress–strain curve, indicating two distinct moduli for cartilage and bone regions, the grafts exhibited single-slope stress–strain behavior up to failure [32]. These results suggest that mechanical strength varies with the different hydrogel concentrations and HAp content within the grafts. Additionally, the discrepancy between the mechanical properties of the graft and the native OC tissue, indicating the functionality of the graft, can be improved by material optimization, crosslinking strategies, and hybrid scaffold approaches [33]. A clinically relevant graft can be formed using these methods. The mechanical properties of the graft may also be improved by embedding cells, which synthesize tissue-related components [34].

Mineral gradients in OC scaffolds and grafts using unitary structures have been developed. For example, Erisken et al. [7] and Liu et al. [35] used electrospinning to

successfully produce thin membranes with mineral gradient thicknesses of 350 and 460 μm, respectively. Mohan et al. [36], Singh et al. [37], and Harley et al. [38] developed unitary scaffolds with graded concentrations of minerals and biomolecules but did not specify the gradient transition lengths. They used microparticles ranging from 100 to 300 μm to form gradients; thus, their gradient transition lengths may have significantly exceeded 700 μm. Levingstone et al. [39], Khanarian et al. [34], and Erickson et al. [32] established gradients with transition lengths exceeding 1 mm. In our study, the thickness of the native OC interface gradient was approximately 140 μm, based on the median values in the violin plot, and approximately 275 μm, based on the mean values in the scatter plot. The reported thickness of the bovine OC interface was approximately 150 μm [40]. We successfully achieved a gradient transition length of (647±21) μm, as determined by TGA, in a unitary graft tailored for OC interface repair and regeneration. This narrow gradient transition length closely mirrors the natural OC interface.

In this study, different methods yielded different gradient thicknesses for the OC tissue specimens. Using TGA, the specimens had to be kept wet, and dehydration inevitably occurred before placing the specimen into the instrument's chamber, causing deviations. Considering the low weight of the specimen (1–2 mg slices were needed to detect the gradual changes), evaporation of water from the native tissue may have introduced significant errors. In addition, TGA is an indirect method of measuring changes in mineral concentrations across the thickness of the OC interface. Therefore, we also evaluated the mineral gradient using EDX, a direct method. This method yielded a mean graft gradient thickness of around 275 μm. The thickness of the graft gradient was approximately 650 μm using either TGA or EDX. To the best of our knowledge, this value is still the lowest mineral gradient thickness generated in a scaffold/graft.

Of note, the optimization parameters were studied in more detail by changing each process parameter over a range while maintaining the other parameters to obtain the lowest possible gradient thickness. The initial parametric study, involving the processing parameters provided in Table 1, showed that the lag time (the time between the incremental change in feed rates) was the dominating parameter. When this parameter was decreased to zero, variations in other parameters had only minimal effects. Thus, the extruder was run at 75 r/min, with a 2 mm×2 mm die opening while instantly changing the feed rates, as described in Table 1 and Fig. 6.

The bone and cartilage layers in the OC tissue contain different densities of cells, which depend on the location. The mean cell density in cartilage is around 9.5×10^6 chondrocytes/mL [41]. Cell density varies more based on the location in the bone. Therefore, the cell count per bone area or thickness is usually reported. Subchondral bone tissue has a cell density of approximately 1.7×10^6 osteoblasts/mL [42, 43]. In this study, the cell density in both cartilage and bone areas was set to the same value of 3×10^4. Thus, there is a three-order-of-magnitude difference in cell numbers for the two zones of the graft compared with native tissues. Our major goal was to mimic the gradient in native OC tissue using a novel bioextrusion methodology. Cells were included as proof of concept for using the extruder as a bioextruder. We believe that using the extruder as a processing tool will support the generation of gradients in scaffolds for OC tissue applications and other applications involving gradients (tendon–bone, ligament–bone, meniscus–bone, muscle–tendon, and other tissue–tissue interfaces).

The bioextrusion of chondrocytes and hFOBs into designated zones produced a graft that physiologically resembled native OC tissue, and cell viability was confirmed after bioextrusion. This accomplishment underscores the efficacy of the bioextrusion technique to produce functionally graded grafts suitable for OC tissue engineering. Moreover, the extrusion method can be scaled up for precision manufacturing, enhancing its applicability in clinical settings. Around 40% of the cells survived the harsh conditions formed by the tight clearances between the screws themselves and between the screws and the wall of the extruder. Cell survival was evaluated in vitro as a function of agarose concentration before feeding the solutions into the extruder. Cell survival peaked at 1.5% agarose and then diminished with further increase in agarose concentration. To optimize the mechanical properties of the gel, a 2% agarose concentration was selected to produce the grafts. Extruders have been used to produce acellular scaffolds, but, to our knowledge, this is the first time an extruder was used as a bioextruder. Cell survival may be optimized by carefully controlling the material and processing conditions. For example, the temperature was maintained at 37.5 °C using an oil bath. However, the temperature within the extruder may have exceeded 37.5 °C due to fluctuations, leading to permanent cell damage. Tighter temperature control may improve cell survival. Other process parameters (screw rotational speed, material feed rate and frequency, and die opening) were controlled to create a gradient with the smallest possible distance, and may not be altered for cell survival without sacrificing the structural changes in the graft. The mechanical properties of hydrogel scaffolds play a significant role in cell survival. Cells survive better in gels with a lower modulus [44]. The modulus of the gel is already low enough and should not be modified to increase cell survival. However, this is a proof-of-concept study to replicate the distribution of minerals at the OC interface, and our future efforts will focus on improving cell survival and functionality.

Our future research will focus on culturing the bioextruded chondrocytes and hFOBs to monitor matrix formation and to analyze the ECM synthesis by the cells. This research will deepen our understanding of graft behavior in a physiological environment and the potential of these grafts for clinical applications.

5 Conclusions

This investigation aimed to develop unitary synthetic OC grafts that replicate the structural properties of native OC tissue using an innovative bioextrusion technique. Our novel application of precise bioextrusion to create a mineral gradient mimicking natural OC interfaces addresses a key challenge in regenerative tissue engineering. Our primary goal was to fabricate grafts that closely match native OC tissue, in terms of mineral gradient transition lengths and viscoelastic properties, and support viable chondrocytes and hFOB cells within their matrix. The use of bioextrusion to achieve narrow gradient transition lengths and integrate living cells directly into the grafts is a novel aspect of this research, pushing the boundaries of current tissue engineering technologies.

One significant challenge was replicating the complex viscoelastic behavior and precise mineral gradients of natural OC tissue. This was addressed by controlling the extrusion of agarose and HAp to fine-tune the material properties and gradient transition lengths. Additionally, ensuring cell viability post-bioextrusion was critical and was successfully managed by optimizing the bioextrusion parameters to maintain a conducive environment for cell survival and integration.

Several steps are necessary to advance the clinical application of these novel bioextruded grafts. The biomechanical properties of the grafts should be enhanced to match or exceed the properties of native tissues. Different material compositions or hybrid structures that incorporate both synthetic and natural materials may be applied to enhance the biomechanical properties. In addition, long-term in vivo studies are essential to assess graft performance, including integration with host tissue, the longevity of the repair, and the functional restoration of joint mechanics.

Transitioning from laboratory-scale bioextrusion to clinically relevant production requires significant advances in automation, reproducibility, and sterility control. The authors have over 40 years of experience with the extrusion process. Thus, automation and reproducibility should not be a significant issue. However, working under sterile conditions with a continuous bioextrusion process (in the presence of cells) presents a significant challenge. Setting up a clean room to perform the entire graft manufacturing process may be necessary.

The economic feasibility of any advanced biomaterial solution is critical. Bioextrusion may reduce costs by integrating gradient fabrication and cell incorporation into a single process. However, sourcing high-purity raw materials, maintaining sterile conditions, and scaling up to clinically relevant batch sizes are challenging. Comparative analyses with existing scaffolds and graft production methods will be an important next step.

In terms of regulatory considerations, these grafts will likely be classified as combination products (device–biologic) by regulatory agencies. Thus, both safety and efficacy must be demonstrated through rigorous preclinical testing, followed by phased clinical trials under Food and Drug Administration/European Medicines Agency (FDA/EMA) guidelines. This requirement emphasizes the need for early engagement with regulatory authorities to align development with approval pathways. Ensuring consistent product quality is paramount. Standardized assessment criteria, requiring the implementation of robust quality management systems and adherence to Good Manufacturing Practice standards for mineral gradient reproducibility, viscoelastic performance, and cell viability, must be developed.

In conclusion, this study sets the groundwork for significant potential advancements in orthopedic treatments by creating grafts that could repair complex OC defects and restore joint function, addressing a critical clinical need that affects millions globally.

Supplementary Information The online version contains supplementary material available at https://doi.org/10.1631/bdm.2500291.

Acknowledgements This research was supported by the School of Engineering and Digital Sciences of Nazarbayev University, Astana, Kazakhstan (to CE).

Author contributions XZ: formal analysis, investigation, methodology, visualization, and writing original draft; WWW: investigation and methodology; XJY: supervision, resources, and review and editing; DMK: conceptualization, methodology, project administration, resources, validation, and review and editing; CE: funding acquisition, conceptualization, methodology, project administration, resources, validation, and review and editing.

Declarations

Conflict of interest The authors declare that they have no conflict of interest.

Ethical approval Ethical approval was not required for this study, as osteochondral tissues were obtained post-mortem from a local abattoir where animals were slaughtered for commercial meat production. No animals were euthanized or handled specifically for research purposes.

Data availability All the data available were submitted with this manuscript.

References

1. Michael JW, Schlüter-Brust KU, Eysel P (2010) The epidemiology, etiology, diagnosis, and treatment of osteoarthritis of the knee. Deutsch Arztebl Int 107(9):152–162. https://doi.org/10.3238/arztebl.2010.0152
2. Langworthy M, Dasa V, Spitzer AI (2024) Knee osteoarthritis: disease burden, available treatments, and emerging options. Ther Adv Musculoskelet Dis 16:1759720X241273009. https://doi.org/10.1177/1759720x241273009
3. MarketsandMarkets (2020) Cartilage Repair Market Report Code BT 4781. https://www.marketsandmarkets.com/Market-Reports/cartilage-repair-regeneration-market-37493272.html [Accessed on 5 May 2025]
4. Gilbert JE (1998) Current treatment options for the restoration of articular cartilage. Am J Knee Surg 11(1):42-46
5. Gadjanski I, Vunjak-Novakovic G (2015) Challenges in engineering osteochondral tissue grafts with hierarchical structures. Expert Opin Biol Ther 15(11):1583–1599. https://doi.org/10.1517/14712598.2015.1070825
6. Lyons TJ, McClure SF, Stoddart RW et al (2006) The normal human chondro-osseous junctional region: evidence for contact of uncalcified cartilage with subchondral bone and marrow spaces. BMC Musculoskelet Disord 7(1):52. https://doi.org/10.1186/1471-2474-7-52
7. Erisken C, Kalyon DM, Wang HJ (2008) Functionally graded electrospun polycaprolactone and β-tricalcium phosphate nanocomposites for tissue engineering applications. Biomaterials 29(30):4065–4073. https://doi.org/10.1016/j.biomaterials.2008.06.022
8. Yildirim N, Amanzhanova A, Kulzhanova G et al (2023) Osteochondral interface: regenerative engineering and challenges. ACS Biomater Sci Eng 9(3):1205–1223. https://doi.org/10.1021/acsbiomaterials.2c01321
9. Kalyon DM, Erisken C, Ozkan S et al (2014) Functionally-graded polymeric graft substitutes and scaffolds for tissue engineering can be fabricated via various extrusion methods. J Tissue Sci Eng 5(1):e128. https://doi.org/10.4172/2157-7552.1000e128
10. Ergun A, Chung R, Ward D et al (2012) Unitary bioresorbable cage/core bone graft substitutes for spinal arthrodesis coextruded from polycaprolactone biocomposites. Ann Biomed Eng 40(5): 1073–1087. https://doi.org/10.1007/s10439-011-0484-1
11. Ergun A, Yu XJ, Valdevit A et al (2012) Radially and axially graded multizonal bone graft substitutes targeting critical-sized bone defects from polycaprolactone/hydroxyapatite/tricalcium phosphate. Tissue Eng Part A 18(23–24):2426–2436. https://doi.org/10.1089/ten.tea.2011.0625
12. Ergun A, Yu XJ, Valdevit A et al (2011) In vitro analysis and mechanical properties of twin screw extruded single-layered and coextruded multilayered poly(caprolactone) scaffolds seeded with human fetal osteoblasts for bone tissue engineering. J Biomed Mater Res Part A 99A(3):354–366. https://doi.org/10.1002/jbm.a.33190
13. Ozkan S, Kalyon DM, Yu XJ (2010) Functionally graded β-TCP/PCL nanocomposite scaffolds: in vitro evaluation with human fetal osteoblast cells for bone tissue engineering. J Biomed Mater Res Part A 92A(3):1007–1018. https://doi.org/10.1002/jbm.a.32425
14. Ozkan S, Kalyon DM, Yu XJ et al (2009) Multifunctional protein-encapsulated polycaprolactone scaffolds: fabrication and in vitro assessment for tissue engineering. Biomaterials 30(26):4336–4347. https://doi.org/10.1016/j.biomaterials.2009.04.050
15. Erisken C, Kalyon DM, Wang HJ (2008) A hybrid twin screw extrusion/electrospinning method to process nanoparticle-incorporated electrospun nanofibres. Nanotechnology 19(16): 165302. https://doi.org/10.1088/0957-4484/19/16/165302
16. Erisken C, Kalyon DM, Wang HJ et al (2011) Osteochondral tissue formation through adipose-derived stromal cell differentiation on biomimetic polycaprolactone nanofibrous scaffolds with graded insulin and beta-glycerophosphate concentrations. Tissue Eng Part A 17(9–10):1239–1252. https://doi.org/10.1089/ten.tea.2009.0693
17. Zhang B, Huang J, Narayan RJ (2020) Gradient scaffolds for osteochondral tissue engineering and regeneration. J Mater Chem B 8:8149–8170. https://doi.org/10.1039/D0TB00688B
18. Mukasheva F, Zhanbassynova A, Erisken C (2024) Biomimetic grafts from ultrafine fibers for collagenous tissues. Bio-Med Mater Eng 35(3):323–335. https://doi.org/10.3233/bme-230193
19. Seitzhaparova B, Timur L, Mirasbek B et al (2025) Rabbit heart bioartificial tissue: perfusion decellularization and characterization. Biomed Phys Eng Express 11(1):015033. https://doi.org/10.1088/2057-1976/ad99de
20. Mauck RL, Soltz MA, Wang CC et al (2000) Functional tissue engineering of articular cartilage through dynamic loading of chondrocyte-seeded agarose gels. J Biomech Eng 122(3): 252–260. https://doi.org/10.1115/1.429656
21. Jiang J, Tang A, Ateshian GA et al (2010) Bioactive stratified polymer ceramic-hydrogel scaffold for integrative osteochondral repair. Ann Biomed Eng 38(6):2183–2196. https://doi.org/10.1007/s10439-010-0038-y
22. Ng KW, Lima EG, Bian LM et al (2010) Passaged adult chondrocytes can form engineered cartilage with functional mechanical properties: a canine model. Tissue Eng Part A 16(3): 1041–1051. https://doi.org/10.1089/ten.TEA.2009.0581
23. Liu YX, Weng RR, Wang WH et al (2020) Tunable physical and mechanical properties of gelatin hydrogel after transglutaminase crosslinking on two gelatin types. Int J Biol Macromol 162:405–413. https://doi.org/10.1016/j.ijbiomac.2020.06.185
24. Guo C, Wu JC, Zeng YM et al (2023) Construction of 3D bioprinting of HAP/collagen scaffold in gelation bath for bone tissue engineering. Regen Biomater 10:rbad067. https://doi.org/10.1093/rb/rbad067
25. Malik M, Kalyon DM, Golba JC Jr (2014) Simulation of co-rotating twin screw extrusion process subject to pressure-dependent wall slip at barrel and screw surfaces: 3D FEM analysis

for combinations of forward- and reverse-conveying screw elements. Int Polym Process 29(1):51–62. https://doi.org/10.3139/217.2802
26. Malik M, Kalyon DM (2022) 3D finite element simulation of processing of generalized Newtonian fluids in counter-rotating and tangential TSE and die combination. Int Polym Process 20(4):398–409. https://doi.org/10.1515/ipp-2005-0068
27. Lawal A, Kalyon DM (1995) Mechanisms of mixing in single and co-rotating twin screw extruders. Polym Eng Sci 35(17): 1325–1338. https://doi.org/10.1002/pen.760351702
28. Kalyon DM, Sangani HN (1989) An experimental study of distributive mixing in fully intermeshing, co-rotating twin screw extruders. Polym Eng Sci 29(15):1018–1026. https://doi.org/10.1002/pen.760291508
29. Erisken C, Kalyon DM, Wang HJ (2010) Viscoelastic and biomechanical properties of osteochondral tissue constructs generated from graded polycaprolactone and beta-tricalcium phosphate composites. J Biomech Eng 132(9):091013. https://doi.org/10.1115/1.4001884
30. Erisken C, Kalyon DM, Zhou J et al (2015) Viscoelastic properties of dental pulp tissue and ramifications on biomaterial development for pulp regeneration. J Endod 41(10):1711–1717. https://doi.org/10.1016/j.joen.2015.07.005
31. Effanga VE, Akilbekova D, Mukasheva F et al (2024) In vitro investigation of 3D printed hydrogel scaffolds with electrospun tidemark component for modeling osteochondral interface. Gels 10(11):745. https://doi.org/10.3390/gels10110745
32. Erickson AE, Sun JL, Lan Levengood SK et al (2019) Chitosan-based composite bilayer scaffold as an in vitro osteochondral defect regeneration model. Biomed Microdevices 21(2):34. https://doi.org/10.1007/s10544-019-0373-1
33. Luo TY, Tan BW, Zhu LJ et al (2022) A review on the design of hydrogels with different stiffness and their effects on tissue repair. Front Bioeng Biotechnol 10:817391. https://doi.org/10.3389/fbioe.2022.817391
34. Khanarian NT, Haney NM, Burga RA et al (2012) A functional agarose-hydroxyapatite scaffold for osteochondral interface regeneration. Biomaterials 33(21):5247–5258. https://doi.org/10.1016/j.biomaterials.2012.03.076
35. Liu F, Mao ZF, Zhang P et al (2018) Functionally graded porous scaffolds in multiple patterns: new design method, physical and mechanical properties. Mater Des 160:849–860. https://doi.org/10.1016/j.matdes.2018.09.053
36. Mohan N, Dormer NH, Caldwell KL et al (2011) Continuous gradients of material composition and growth factors for effective regeneration of the osteochondral interface. Tissue Eng Part A 17(21–22):2845–2855. https://doi.org/10.1089/ten.tea.2011.0135
37. Singh M, Morris CP, Ellis RJ et al (2008) Microsphere-based seamless scaffolds containing macroscopic gradients of encapsulated factors for tissue engineering. Tissue Eng Part C Meth 14(4):299–309. https://doi.org/10.1089/ten.tec.2008.0167
38. Harley BA, Lynn AK, Wissner-Gross Z et al (2010) Design of a multiphase osteochondral scaffold III: fabrication of layered scaffolds with continuous interfaces. J Biomed Mater Res Part A 92A(3):1078–1093. https://doi.org/10.1002/jbm.a.32387
39. Levingstone TJ, Matsiko A, Dickson GR et al (2014) A biomimetic multi-layered collagen-based scaffold for osteochondral repair. Acta Biomater 10(5):1996–2004. https://doi.org/10.1016/j.actbio.2014.01.005
40. Khanarian NT, Boushell MK, Spalazzi JP et al (2014) FTIR-I compositional mapping of the cartilage-to-bone interface as a function of tissue region and age. J Bone Miner Res 29(12): 2643–2652. https://doi.org/10.1002/jbmr.2284
41. Hunziker EB, Quinn TM, Häuselmann HJ (2002) Quantitative structural organization of normal adult human articular cartilage. Osteoarthr Cartilage 10(7):564–572. https://doi.org/10.1053/joca.2002.0814
42. Mohamed AM (2008) An overview of bone cells and their regulating factors of differentiation. Malays J Med Sci 15(1):4–12
43. Pazzaglia UE, Congiu T, Sibilia V et al (2014) Osteoblast-osteocyte transformation. A SEM densitometric analysis of endosteal apposition in rabbit femur. J Anat 224(2):132–141. https://doi.org/10.1111/joa.12138
44. Banerjee A, Arha M, Choudhary S et al (2009) The influence of hydrogel modulus on the proliferation and differentiation of encapsulated neural stem cells. Biomaterials 30(27):4695–4699. https://doi.org/10.1016/j.biomaterials.2009.05.050